

Predictable variations of the carbon sinks and atmospheric CO₂ growth in a multi-model framework

T. Ilyina¹, H. Li¹, A. Spring^{1,2}, W. A. Müller¹, L. Bopp³, M. O. Chikamoto⁴,
G. Danabasoglu⁵, M. Dobrynin⁶, J. Dunne⁷, F. Fransner⁸, P. Friedlingstein⁹,
W. Lee¹⁰, N. S. Lovenduski¹¹, W.J. Merryfield¹⁰, J. Mignot¹², J.Y. Park¹³, R.
Séférian¹⁴, R. Sospedra-Alfonso¹⁰, M. Watanabe¹⁵, S. Yeager⁵

¹Max Planck Institute for Meteorology, Bundesstraße 53, 20146 Hamburg, Germany

²International Max-Planck Research School of Earth System Modelling, Bundesstraße 53, 20146,
Hamburg, Germany

³LMD-IPSL, CNRS, Ecole Normale Supérieure / PSL Res. Univ, Ecole Polytechnique, Sorbonne
Université, Paris, France

⁴Institute for Geophysics, Jackson School of Geosciences, University of Texas at Austin, Austin, Texas
USA

⁵National Center for Atmospheric Research, Boulder, Colorado, USA

⁶Deutscher Wetterdienst (DWD), Hamburg, Germany

⁷NOAA/OAR Geophysical Fluid Dynamics Laboratory, Princeton, NJ 08540 USA

⁸Geophysical Institute, University of Bergen, and Bjerknes Centre for Climate Research, Bergen, Norway

⁹College of Engineering, Mathematics and Physical Sciences, University of Exeter, Exeter EX4 4QF, UK

¹⁰Canadian Centre for Climate Modelling and Analysis, Environment and Climate Change Canada,
Victoria, British Columbia, Canada

¹¹Department of Atmospheric and Oceanic Sciences and Institute of Arctic and Alpine Research,
University of Colorado, Boulder, Colorado, USA

¹²LOCEAN, Sorbonne Universites/IRD/CNRS/MNHN, Paris, France

¹³Department of Earth and Environmental Sciences, Jeonbuk National University, Jeollabuk-do 54896
Republic of Korea

¹⁴CNRM, Université de Toulouse, Météo-France, CNRS, Toulouse, France

¹⁵Research Institute for Global Change, Japan Agency for Marine-Earth Science and Technology
(JAMSTEC), 3173-25, Showa-machi, Kanazawa-ku, Yokohama, Kanagawa, 236-0001, Japan

Corresponding author: Tatiana Ilyina, tatiana.ilyina@mpimet.mpg.de

29

Key Points:

30

- Predictive skill of the global ocean carbon sink due to initialization is up to 6 years, with longer regional predictability in single models.

31

32

- Predictive skill due to initialization for the land carbon sink of up to 2 years is primarily maintained in the tropics and extra-tropics.

33

34

- Anomalies of atmospheric CO₂ growth rate are predictable up to 2 years and are limited by the land carbon sink predictability horizon.

35

Abstract

Inter-annual to decadal variability in the strength of the land and ocean carbon sinks impede accurate predictions of year-to-year atmospheric carbon dioxide (CO₂) growth rate. Such information is crucial to verify the effectiveness of fossil fuel emissions reduction measures. Using a multi-model framework comprising prediction systems based on Earth system models, we find a predictive skill for the global ocean carbon sink of up to 6 years. Longer regional predictability horizons and robust spatial patterns are found across single models. On land, a predictive skill of up to 2 years is primarily maintained in the tropics and extra-tropics enabled by the initialization of the physical climate variables towards observations. We further show that anomalies of atmospheric CO₂ growth rate inferred from natural variations of the land and ocean carbon sinks are predictable at lead time of 2 years and the skill is limited by the land carbon sink predictability horizon.

Plain Language Summary

Variations of the natural land and ocean carbon sinks in response to climate variability strongly regulate year-to-year variations in the growth rate of atmospheric carbon dioxide (CO₂). Information on the near-term evolution of the carbon sinks and CO₂ in the atmosphere is necessary to understand where the anthropogenic carbon would go in response to emission reduction efforts addressing global warming mitigation. Predictions of this near-term evolution would thus assist policy-relevant analysis. Here we use a set of prediction systems based on Earth system models to establish predictive skills of the ocean and land carbon sinks and to infer predictability of atmospheric CO₂ growth rate. We show predictability horizons of up to 6 years for the globally integrated ocean carbon sink in individual models with even higher predictive skill in some models and regions. Variations of the land carbon sink are predictable up to 2 years and limit predictability of changes in atmospheric CO₂ growth rate at lead time of 2 years. Our study demonstrates an emerging capacity of the initialized simulations for skillful predictions of the global carbon sink and atmospheric CO₂ variations.

1 Introduction

On interannual to decadal time-scales, atmospheric CO₂ growth rates exhibit pronounced anomalies driven by varying strengths of the land and ocean carbon sinks; these

67 anomalies are linked to climate variability (Peters et al., 2017; Friedlingstein et al., 2019;
68 Landschützer et al., 2019). Variability in ocean carbon uptake is associated with major
69 carbon uptake regions such as the Southern Ocean and the North Atlantic (Landschützer
70 et al., 2019). Inter-annual variations of the land carbon sink are primarily driven by the
71 terrestrial biosphere response to El Niño Southern Oscillation (ENSO) (Ropelewski &
72 Halpert, 1987; Jones et al., 2001; Zeng et al., 2005; Kim et al., 2016). Year-to-year vari-
73 ations of the air-land carbon flux are about one order of magnitude higher than varia-
74 tions in the air-sea CO₂ fluxes (Doney et al., 2006). Hence, predicted El Niño variabil-
75 ity has been used, in combination with an average CO₂ growth rate due to anthropogenic
76 CO₂ emissions, to predict, from a simple linear regression, the atmospheric CO₂ growth
77 at Mauna Loa for the subsequent year (Betts et al., 2016). Predicting changes in atmo-
78 spheric CO₂ growth rate beyond this horizon remains a major challenge. Such informa-
79 tion will be essential for the evaluation of mitigation efforts in real-time in the presence
80 of internal climate variability in support of policy-relevant analysis for the UNFCCC global
81 stocktakes (UNFCCC, 2015).

82 Recent initialized predictions of near-term future climate have proven successful
83 (Marotzke et al., 2016; Smith et al., 2007) with predictive power of carbon sinks also emerg-
84 ing. Li et al. (2019) established a predictive skill of the globally aggregated air-sea CO₂
85 fluxes of up to 2 years assessed against an observational product. Longer predictability
86 in regions like the North Atlantic and the Southern Ocean is suggested (Li et al., 2016;
87 Lovenduski, Yeager, et al., 2019; Fransner et al., 2020). ESM-based initialized predic-
88 tion systems also demonstrate predictability of other marine biogeochemical properties
89 such as net primary production, export production, and seawater pH (Park et al., 2019;
90 Séférian et al., 2014; Yeager et al., 2018; Brady et al., 2020; Fransner et al., 2020; Krumhardt
91 et al., 2020). On the land side, a potential prediction skill of 2 years was established for
92 terrestrial net ecosystem production (Lovenduski, Bonan, et al., 2019), but only of 9 months
93 for tropical land-atmosphere carbon flux (Zeng et al., 2008). Perfect-model frameworks
94 based on idealized simulations suggest analogous predictability horizons for the carbon
95 sinks (Séférian et al., 2018; Spring & Ilyina, 2020). However, previous studies were ei-
96 ther limited to internally consistent model environments of perfect models (Séférian et
97 al., 2018; Spring & Ilyina, 2020; Frölicher et al., 2020) or single initialized models (Li et
98 al., 2019, 2016; Lovenduski, Yeager, et al., 2019; Yeager et al., 2018; Fransner et al., 2020;

99 Krumhardt et al., 2020). Furthermore, they did not address predictability of variations
100 in atmospheric CO₂ growth.

101 Here, we assess how well different ESM-based initialized prediction systems cap-
102 ture variations of the global land and ocean carbon sinks and their predictability. We
103 make a step further and for the first time examine the resulting predictability of vari-
104 ations in the growth rate of atmospheric CO₂ that is driven by the response of carbon
105 sinks to climate variability. As predictions of carbon sink evolution still remain a cutting-
106 edge activity of only a few modeling groups, a common protocol is not yet available (Merryfield
107 et al., 2020). Our multi-model framework comprises ESM-based prediction systems that
108 contributed to the Decadal Climate Prediction Project (DCPP; Boer et al. (2016)) within
109 the Coupled Model Intercomparison Project Phase 6 (CMIP6), as well as those which
110 run with the CMIP5 forcing. This enables us to establish predictive skills in a larger num-
111 ber of models, whilst performance of CMIP5 and CMIP6 model versions with respect
112 to different aspects of the carbon cycle has been addressed in recent studies (Arora et
113 al., 2019; Séférian et al., 2020; Kwiatkowski et al., 2020). Prediction systems follow some-
114 what different initialization techniques and data assimilation methods based on the "best
115 effort" of the different modeling centers. This approach arises from the overall DCPP
116 philosophy of not specifying single details of the implementation and design of the multi-
117 model predictions and thereby encompass aspects of the inherent uncertainty of climate
118 predictions (Boer et al., 2016).

119 **2 Materials and Methods**

120 We use a multi-model framework comprising several ESM-based prediction systems,
121 including CanESM5 (Swart et al., 2019), CESM-DPLE (Yeager et al., 2018), GFDL-ESM2
122 (Park et al., 2018), IPSL-CM6A-LR (Boucher et al., 2020), MIROC-ES2L (Watanabe
123 et al., 2020), MPI-ESM-LR (Giorgetta et al., 2013), MPI-ESM1.2-HR (Mauritsen et al.,
124 2019), and NorCPM1 (Counillon et al., 2016). Details of each prediction system are given
125 in Supporting Information. Simulations with CanESM5, IPSL-CM6A-LR, MIROC-ES2L,
126 MPI-ESM1.2-HR, and NorCPM1 contributed to CMIP6 DCPP following historical forc-
127 ing until 2014 and climate change scenario SSP2-4.5. Simulations with CESM-DPLE,
128 GFDL-ESM2, and MPI-ESM-LR were performed under CMIP5 historical forcing un-
129 til the year 2005 and followed either RCP4.5 (GFDL-ESM2, MPI-ESM-LR) or RCP8.5
130 (CESM-DPLE) climate change scenario thereafter.

131 The ensemble size in single prediction systems ranges between at least 10 members
132 for most of the models up to 40 for CESM-DPLE (Table S1), enabling us to demonstrate
133 the added value of a larger ensemble. For NorCPM1, we merged the two decadal hind-
134 cast products with 10 members each, producing one ensemble of 20 members. In the MPI-
135 ESM based systems, only the lower resolution MPI-ESM-LR included both the land and
136 the ocean biogeochemistry components. MPI-ESM1.2-HR was configured with a higher
137 resolution in the atmosphere and ocean, but did not integrate the land biogeochemistry
138 component.

139 In all models the carbon cycle components are only indirectly initialized with the
140 data assimilative physics. Hence, we assess observed variability in carbon sinks captured
141 through initialization of prediction systems by the observed state of the physical climate.
142 All simulations ran with prescribed evolution of atmospheric CO₂ concentrations and
143 land use change.

144 We present three types of simulations. Reconstruction simulations include observed
145 signals of climate variability introduced by assimilative observed and reanalysis prod-
146 ucts over a hindcast period. Uninitialized simulations are based on continuous histor-
147 ical simulations following CMIP6 or CMIP5 forcing (not the observed signals), i.e. the
148 model physics evolves independently and the resulting climate variability does not nec-
149 essarily match the observed one. Initialized simulations are retrospective prediction sim-
150 ulations that start from a respective reconstruction simulations and develop internal cli-
151 mate variability that may be out of phase with observed climate variability. We com-
152 pare the initialized simulations against the uninitialized ones to assess predictive skill
153 that is established due to initialization. This predictive skill is characterized by the anomaly
154 correlation coefficients (ACC) between the model simulations and different reference data
155 products. The anomalies are calculated by removing the climatological mean for the re-
156 construction and uninitialized simulations, and for the initialized simulations with ad-
157 ditionally respect to the lead time. Note that we present the improved predictive skill
158 due to initialization based on the comparison of ACC in the initialized predictions rel-
159 ative to that in the uninitialized simulations. We use a bootstrapping resample method
160 to quantify the significance of the improved predictive skill (Li et al., 2019). The spa-
161 tial map of predictive skill and the corresponding significance is generated by the cen-
162 tral evaluation system MurCSS, which is a commonly used evaluation tool in decadal
163 predictions (Illing et al., 2014). The focus time period of this study is from 1982-2013,

164 when the global carbon cycle experienced large interannual to decadal variations. The
165 time series are all linearly detrended to emphasize the predictability in interannual to
166 decadal variability. The global time series are integrated based on the original model grid.
167 For the spatial pattern of ACC calculation, the variables are conservatively interpolated
168 into 5 degree.

169 For land carbon uptake, direct observational estimates capturing the regional and
170 global temporal variability are not available, hence we use the Global Carbon Budget
171 2019 (GCB; Friedlingstein et al. (2019)) carbon sinks estimate as a benchmark. Under-
172 going annual updates, GCB offers a comprehensive and temporally consistent time-series
173 of stand-alone land and ocean carbon cycle model simulations forced with observed cli-
174 mate data or climate reanalysis and additional observational products (atmospheric CO₂,
175 land cover change, etc.). For ocean carbon uptake, we additionally use the SOM-FFN
176 (Landschützer et al., 2015) observationally based product. In addition, the HadISST data
177 (Rayner et al., 2003) is used to compare with model simulations of sea surface temper-
178 ature and to calculate the ENSO index.

179 **3 Variations of ocean and land carbon sinks in initialized simulations**

180 First we examine the ability of reconstructions and initialized predictions to sim-
181 ulate observed interannual variations in carbon sinks. Both reconstructions and initial-
182 ized predictions at lead time of 2 years appropriately capture multi-year variations of the
183 anomalous air-sea flux of CO₂ represented in the GCB and data-based SOM-FFN es-
184 timates (Fig.1 left). The uninitialized simulations mostly capture only ocean carbon sink
185 increases in response to rising carbon emissions and thus follow a smoother temporal evo-
186 lution. Furthermore, reconstructions suggest stronger multi-year variations in the ocean
187 carbon sink and outperform the uninitialized simulations in GFDL-ESM2, MIROC-ES2L,
188 MPI-ESM1.2-HR, and in NorCPM1 (only in comparison to SOM-FFN data). Lower cor-
189 relations of reconstruction simulations as opposed to the uninitialized ones in CanESM5,
190 IPSL-CM6A-LR, and MPI-ESM-LR can be related to two aspects of the design of our
191 analysis. First, the assimilation techniques may not be optimally calibrated to represent
192 ocean biogeochemistry in reconstruction (Park et al., 2018; Li et al., 2019). Second, GCB
193 and SOM-FFN estimates chosen as the reference here are prone to their own uncertain-
194 ties. GCB estimates are essentially an average of various stand-alone hindcast model sim-
195 ulations. The neural network approach of SOM-FFN is limited by spatial and tempo-

196 ral gaps in observations. While the different model outputs show a large spread in air-
197 sea CO₂ flux, they overall fall within the range of the SOCOM data products (Rödenbeck
198 et al., 2015). The weakening ocean carbon sink captured in the SOM-FFN data prod-
199 uct in the 1990s is revealed by the stronger negative trends in the reconstruction and ini-
200 tialized simulations vs. the uninitialized ones, which are more pronounced in some pre-
201 diction systems (in MPI-ESM-LR, MPI-ESM-HR, MIROC-ES2L, and partially in GFDL-
202 ESM2). Other models (CanESM5, CESM-DPLE, NorCPM1, IPSL-CM6A-LR) capture
203 a lower amplitude of the weakened ocean carbon sink, more consistent with the GCB
204 estimate. Starting from the beginning of the 21st century, reconstruction simulations show
205 an enhancement of the ocean carbon uptake with a stronger increase in the ocean car-
206 bon sink at the beginning of the 21st century as compared to the uninitialized ones. This
207 decadal shift in evolution of the ocean carbon sink at the onset of the 21st century is at-
208 tributable to climate modulated variability and is consistent with the SOM-FFN data
209 estimate (Landschützer et al., 2015).

210 The fewer land carbon reconstruction simulations available to us all outperform the
211 uninitialized simulations in capturing the major year-to-year variations as indicated by
212 higher correlations with GCB (Fig.1 right). This correlation skill with the GCB estimates
213 is maintained at lead year 2. Unsurprisingly, uninitialized simulations do not capture the
214 timing of air-land CO₂ flux variations. Response to the warm and cold episodes of ENSO,
215 the major driver of year-to-year variability of the air-land carbon fluxes, is clearly man-
216 ifested in the GCB estimates and reconstructions (Fig. S1). It is notable that air-land
217 CO₂ flux in CanESM5 has the highest correlation with GCB in reconstruction simula-
218 tion, supported by the highest of all models correlation in the uninitialized simulation
219 (Fig.1d). For NorCPM1 and MPI-ESM-LR assimilation data helps to establish corre-
220 lation in reconstruction simulations. While there has been some progress in global mod-
221 els over the past decades (Bellenger et al., 2014), representing ENSO still remains a ma-
222 jor challenge. Yet, a major improvement in the reconstruction simulations with respect
223 to air-land CO₂ flux, gives us confidence that initialized prediction systems capture the
224 important processes that link the land carbon cycle to ENSO. The reconstruction sim-
225 ulations produce a distinct weakening of the land carbon uptake in response to major
226 El Niño events, followed by a strong increase in the land carbon sink during La Niña events.
227 These variations are not captured in the uninitialized simulations as they are not in phase
228 with the observed climate variability.

4 Predictability of carbon sinks and atmospheric CO₂ growth rate

We next examine effects of the global land ocean carbon sink variations on the inferred variability and predictability of atmospheric CO₂ growth rate (Fig.2). Note that all prediction systems available to us are forced with prescribed evolution of atmospheric concentrations of CO₂ (rather than with prescribed emissions of CO₂) and so the atmospheric compartments of those models do not respond to land or ocean CO₂ fluxes. Here, the detrended sum of the global land and ocean carbon fluxes serves as a diagnostic of variations in the temporal evolution of the atmospheric CO₂ growth driven by climate modulated variability of carbon sinks. These variations of a few PgC in the reconstruction simulations generally follow the evolution inferred from the GCB estimate (Fig.2a).

We find predictability of variations in atmospheric CO₂ growth at lead times of 2 years in most models, as indicated by higher correlations with GCB of the initialized simulations in comparison to the uninitialized ones (Fig.2 b, c). Given the higher amplitude of interannual air-land CO₂ flux variability, atmospheric carbon growth rate anomalies predominantly follow the land carbon sink evolution, and the ocean carbon sink acts to dampen the land modulated interannual variations of atmospheric CO₂ (Doney et al., 2006; Lee et al., 1998). Indeed, the improved correlation skill of air-land CO₂ fluxes with the GCB estimates is maintained at lead year 2 and outperforms the uninitialized simulations in all models except MIROC-ES2L (Fig.1f).

We further assess predictability horizons of the global ocean and land carbon sinks, as well as of the diagnosed changes in atmospheric CO₂ growth represented by the lead years with improved predictive skill due to initialization (Fig.3). Predictive skill of the ocean carbon sink significantly improves with initialization up to lead year 5 against the SOM-FFN data product in MPI-ESM1.2-HR and up to lead year 6 in CESM-DPLE and NorCPM1, respectively (Fig.3a). The predictive skill of CESM-DPLE is higher than reported in a previous study (Lovenduski, Yeager, et al., 2019) mainly because we focus on a different time period and use the SOM-FFN observationally based estimates rather than reconstruction here. A larger ensemble size of CESM-DPLE relative to the outputs from the other prediction systems maintains the predictive skill significance. Considering fewer ensemble members degrades its predictive skill significance (as indicated by the p-value dependence on ensemble size; Fig. S2). A previous study (Li & Ilyina, 2018) suggests that a large ensemble size is needed to capture decadal variations in the ocean car-

261 bon sink. Therefore, an increased ensemble prediction size could enhance the predictive
262 skill of global carbon fluxes in other prediction systems, as well as in a multi-model en-
263 semble.

264 Predictive skill due to initialization up to lead year 2 for land carbon sink verified
265 against GCB estimates is found in CanESM5, IPSL-CM6A-LR, MPI-ESM, and NorCPM1
266 (Fig.3b). This skill, supported by higher coherence between GCB estimates and initial-
267 ized simulations at lead time of 2 years in most models (Fig.1f), goes well beyond a sea-
268 sonal skill attainable in previous studies. A slightly lower and insignificant skill was found
269 for CESM-DPLE because of the initialization of atmosphere and land from a random
270 ensemble member of CESM-LE (see Materials and Methods and Lovenduski, Bonan, et
271 al. (2019)).

272 The atmospheric CO₂ growth rate changes induced by land and ocean carbon sink
273 variations show predictive skill to lead year 2 (Fig.3) in the same models which have sig-
274 nificant 2 year predictive horizons for the land carbon sink (i.e. in CanESM5, IPSL-CM6A-
275 LR, MPI-ESM, and NorCPM1). Given the longer predictive horizons of the ocean car-
276 bon sink, our results indicate that predictability of the atmospheric CO₂ growth in these
277 models is limited by the land carbon sink predictability. Analogously, a previous study,
278 based on a perfect model framework (Spring & Ilyina, 2020), demonstrates that the pre-
279 dictive skill of atmospheric CO₂ concentration of 3 years is dampened by land.

280 **5 Spatial patterns of predictability horizons of CO₂ fluxes**

281 The prediction systems use different initialization techniques and data assimilation
282 methods, but do they establish robust spatial patterns of predictability horizons in the
283 carbon cycle? To address this question we examine predictability horizons due to added
284 value of initialization, represented by the lead years when correlations of the initialized
285 simulations are larger than those in the uninitialized ones. We find overall rather con-
286 sistent CO₂ flux predictability horizons established due to initialization in the different
287 prediction systems (Fig.4).

288 In some ocean regions, the improved skill is retained for up to 9-10 years, thereby
289 going beyond the predictability horizons of the physical climate variables (Séférian et
290 al., 2014; Li et al., 2016). We find regional improvements in air-sea CO₂ flux predictabil-
291 ity due to initialization (as indicated by the difference between the initialized and unini-

292 tialized simulations and consistent spatial patterns of predictive skill at lead year 2 across
293 models shown in Fig. S3-S4). These improved regions differ across the models and when
294 assessing them vs. the GCB estimates or the SOM-FFN (Fig. S3) and the reconstruc-
295 tions (Fig. S4), highlighting the importance of high-quality reference for skillful predic-
296 tions of the ocean carbon sink. The air-sea CO₂ flux dynamics is regulated by the tem-
297 poral gradient of surface ocean pCO₂. Because of the fast equilibration of CO₂ between
298 atmosphere and surface ocean in most areas, pCO₂ tracks atmospheric CO₂ evolution.
299 This feature is fairly well captured in ocean biogeochemical models (Roy et al., 2011).
300 Furthermore, our previous findings (Li et al., 2019) suggest that temperature variations
301 largely control shorter-term (<3 years) predictability of the ocean carbon sink, while longer-
302 term (>3 years) predictability is associated with nonthermal drivers. Coherent repre-
303 sentation of the spatial patterns of the air-sea CO₂ flux in the different prediction sys-
304 tems may be driven by the robust representation of SST variations in the initialized pre-
305 dictions considered here (Fig. S5).

306 On the land side, statistically significant improvements due to initialization (in CanESM5,
307 IPSL-CM6A-LR, MPI-EMS-LR, and NorCPM1) are suggested in regions of the trop-
308 ics (e.g. Amazon, West Africa) and extra-tropics (e.g. Middle East, US Great Plains,
309 Eastern Russia). These prediction systems represent land carbon fluxes improved due
310 to initialization at lead time of 2 years. Less pronounced predictive skill of land carbon
311 fluxes is found in CESM-DPLE due to the initialization of atmosphere and land from
312 a random ensemble member; see Materials and Methods and Lovenduski, Bonan, et al.
313 (2019)).

314 **6 Conclusions**

315 One major requirement related to the goal of the Paris Agreement of "limiting warm-
316 ing to well below 2°C, and pursuing efforts to 1.5°C", is to discern the pathways of an-
317 thropogenic carbon in the Earth system in order to verify the effectiveness of fossil fuel
318 emissions reduction measures. A major scientific challenge in this context will be to pre-
319 dict the inter-annual and decadal variations of the natural carbon sinks and the related
320 variations in the growth rate of atmospheric CO₂, as well as their susceptibility to on-
321 going climate change. Thus, predictability of variations of the global carbon cycle is a
322 crucial emerging topic requiring fast advance as it relates to the global stocktaking re-
323 quirements of the Paris Agreement.

324 Here we provide a first multi-model assessment of the initialized carbon cycle pre-
325 dictions, which is an important step towards skillful near-term predictions of the evo-
326 lution of the land and ocean carbon sinks and the resulting variations in atmospheric CO₂
327 growth in response to climate variability and changes in anthropogenic carbon emissions.
328 We find improved predictive skill due to initialization in both ocean and land carbon sinks.
329 Predictive skill due to initialization for the global air-sea CO₂ flux is up to 6 years. There
330 is indication of even higher regional skill in single models and regions. Representation
331 of air-land CO₂ flux improved due to initialization in all models considered in this study.
332 We demonstrate predictive horizons of up to 2 years in 4 out of the 6 models considered
333 in this study. As year-to-year variations in atmospheric CO₂ are largely determined by
334 variations of the land carbon sink, the predictability horizon of 2 years found for the at-
335 mospheric CO₂ growth rate is maintained by predictability of air-land CO₂ flux.

336 Ongoing challenges in predictions of the global carbon cycle include a lack of ob-
337 servationally based products suitable to initialize the ESMs and to verify prediction skill,
338 the unavailability of standardized multi-model simulations that include prognostic car-
339 bon cycle components, and the insufficient prediction ensemble size that impairs signif-
340 icance assessment. Despite these challenges, our analysis provides clear indications that
341 further advancement of the physical and biogeochemical components of prediction sys-
342 tems and larger ensembles could timely address some of these challenges as new predic-
343 tion simulations and updated observational products become available. Our analysis demon-
344 strates an emerging capacity of the initialized simulations for skillful predictions of the
345 carbon cycle. Thus, such multi-model initialized predictions would offer a powerful tool
346 in support of governmental and economical decisions related to verification and efficiency
347 assessment of near-term carbon emission reduction pathways.

348 **Acknowledgments**

349 Funding: T.I., H.L., W.A.M. were supported by the Federal Ministry of Education and
350 Research in Germany (BMBF) through the research program MiKlip (grant no. 01LP1517B).
351 T.I., P.F., H.L., L.B., R.S. were supported by the European Union's Horizon 2020 re-
352 search and innovation program under grant agreement no. 641816 (CRESCENDO). T.I.,
353 P.F., H.L. L.B. were supported by the European Union's Horizon 2020 research and in-
354 novation program under grant agreement no. 821003 (4C). R.S. was supported by the
355 TRIATLAS project under grant agreement no. 817578. N.S.L. was supported by the U.S.

356 National Science Foundation (OCE-1752724). F.F. was supported by the Nansen Legacy
357 Project (276730) and Det Kongelige Norske Videnskabers Selskap. M.C. was supported
358 by National Science Foundation (OCE-1635465) and grant-in-aid for Scientific Research
359 on Innovative Areas (15H05817). J.-Y.P. was supported by NOAA's marine ecosystem
360 tipping points initiative and the National Research Foundation of Korea (NRF-2020R1A4A3079510).
361 M.W. was supported by the Integrated Research Program for Advancing Climate Mod-
362 els (TOUGOU) Grant Number JPMXD0717935457 and JPMXD0717935715 from the
363 Ministry of Education, Culture, Sports, Science and Technology (MEXT), Japan. The
364 National Center for Atmospheric Research (NCAR) is a major facility sponsored by the
365 US National Science Foundation (NSF) under Cooperative Agreement No. 1852977. Sim-
366 ulations with MPI-ESM were performed at the German Climate Computing Center (DKRZ).
367 The CESM-DPLE was generated using computational resources provided by the National
368 Energy Research Scientific Computing Center, which is supported by the Office of Sci-
369 ence of the US Department of Energy under contract no. DEAC02-05CH11231, as well
370 as by an Accelerated Scientific Discovery grant for Cheyenne (<https://doi.org/10.5065/D6RX99HX>)
371 that was awarded by NCAR's Computational and Information Systems Laboratory. Pri-
372 mary data and scripts used in the analysis of this study are archived by the Max Planck
373 Institute for Meteorology and can be obtained by contacting publications@mpimet.mpg.de.

374 References

- 375 Arora, V. K., Katavouta, A., Williams, R. G., Jones, C. D., Brovkin, V., Friedling-
376 stein, P., ... Ziehn, T. (2019). Carbon-concentration and carbon-
377 climate feedbacks in CMIP6 models, and their comparison to CMIP5 mod-
378 els. *Biogeosciences Discussions*, 2019, 1–124. Retrieved from [https://](https://bg.copernicus.org/preprints/bg-2019-473/)
379 bg.copernicus.org/preprints/bg-2019-473/ doi: 10.5194/bg-2019-473
- 380 Bellenger, H., Guilyardi, É., Leloup, J., Lengaigne, M., & Vialard, J. (2014). ENSO
381 representation in climate models: From CMIP3 to CMIP5. *Climate Dynamics*,
382 42(7-8), 1999–2018.
- 383 Betts, R. A., Jones, C. D., Knight, J. R., Keeling, R. F., & Kennedy, J. J. (2016). El
384 Niño and a record CO₂ rise. *Nature Climate Change*, 6(9), 806–810.
- 385 Boer, G. J., Smith, D. M., Cassou, C., Doblas-Reyes, F., Danabasoglu, G., Kirt-
386 man, B., ... others (2016). The decadal climate prediction project (DCPP)
387 contribution to CMIP6. *Geoscientific Model Development (Online)*, 9(10).

- 388 Boucher, O., Servonnat, J., Albright, A. L., Aumont, O., Balkanski, Y., Bastrikov,
389 V., ... others (2020). Presentation and evaluation of the IPSL-CM6A-LR
390 climate model. *Journal of Advances in Modeling Earth Systems*, 12(7).
- 391 Brady, R. X., Lovenduski, N. S., Yeager, S. G., Long, M. C., & Lindsay, K. (2020).
392 Skillful multiyear predictions of ocean acidification in the California current
393 system. *Nature Communications*, 11(1), 1–9.
- 394 Counillon, F., Keenlyside, N., Bethke, I., Wang, Y., Billeau, S., Shen, M. L., &
395 Bentsen, M. (2016). Flow-dependent assimilation of sea surface tem-
396 perature in isopycnal coordinates with the Norwegian Climate Prediction
397 Model. *Tellus A: Dynamic Meteorology and Oceanography*, 68(1), 32437.
398 Retrieved from <https://doi.org/10.3402/tellusa.v68.32437> doi:
399 10.3402/tellusa.v68.32437
- 400 Doney, S. C., Lindsay, K., Fung, I., & John, J. (2006). Natural variability in a
401 stable, 1000-yr global coupled climate–carbon cycle simulation. *Journal of*
402 *climate*, 19(13), 3033–3054.
- 403 Fransner, F., Counillon, F., Bethke, I., Tjiputra, J., Samuelsen, A., Nummelin, A., &
404 Olsen, A. (2020). Ocean biogeochemical predictions—initialization and limits
405 of predictability. *Frontiers in Marine Science*, 7, 386.
- 406 Friedlingstein, P., Jones, M., O’sullivan, M., Andrew, R., Hauck, J., Peters, G., ...
407 others (2019). Global carbon budget 2019. *Earth System Science Data*, 11(4),
408 1783–1838.
- 409 Frölicher, T. L., Ramseyer, L., Raible, C. C., Rodgers, K. B., & Dunne, J. (2020).
410 Potential predictability of marine ecosystem drivers. *Biogeosciences*, 17, 2061-
411 2083.
- 412 Giorgetta, M. A., Jungclaus, J., Reick, C. H., Legutke, S., Bader, J., Böttinger, M.,
413 ... others (2013). Climate and carbon cycle changes from 1850 to 2100 in
414 MPI-ESM simulations for the Coupled Model Intercomparison Project phase 5.
415 *Journal of Advances in Modeling Earth Systems*, 5(3), 572–597.
- 416 Illing, S., Kadow, C., Oliver, K., & Cubasch, U. (2014). Murcss: A tool for stan-
417 dardized evaluation of decadal hindcast systems. *Journal of Open Research*
418 *Software*, 2(1).
- 419 Jones, C. D., Collins, M., Cox, P. M., & Spall, S. A. (2001). The carbon cycle re-
420 sponse to ENSO: A coupled climate–carbon cycle model study. *Journal of Cli-*

- 421 *mate*, 14(21), 4113–4129.
- 422 Kim, J.-S., Kug, J.-S., Yoon, J.-H., & Jeong, S.-J. (2016). Increased atmospheric CO₂
423 growth rate during El Niño driven by reduced terrestrial productivity in the
424 CMIP5 ESMs. *Journal of Climate*, 29(24), 8783–8805.
- 425 Krumhardt, K. M., Lovenduski, N. S., Long, M. C., Luo, J. Y., Lindsay, K., Yeager,
426 S., & Harrison, C. (2020). Potential predictability of net primary production
427 in the ocean. *Global Biogeochemical Cycles*, 34, e2020GB006531.
- 428 Kwiatkowski, L., Torres, O., Bopp, L., Aumont, O., Chamberlain, M., Christian,
429 J. R., . . . others (2020). Twenty-first century ocean warming, acidification,
430 deoxygenation, and upper-ocean nutrient and primary production decline from
431 CMIP6 model projections. *Biogeosciences*, 17(13), 3439–3470.
- 432 Landschützer, P., Gruber, N., Haumann, F. A., Rödenbeck, C., Bakker, D. C.,
433 Van Heuven, S., . . . others (2015). The reinvigoration of the southern ocean
434 carbon sink. *Science*, 349(6253), 1221–1224.
- 435 Landschützer, P., Ilyina, T., & Lovenduski, N. S. (2019). Detecting regional modes
436 of variability in observation-based surface ocean pCO₂. *Geophysical Research*
437 *Letters*, 46(5), 2670–2679.
- 438 Lee, K., Wanninkhof, R., Takahashi, T., Doney, S. C., & Feely, R. A. (1998). Low
439 interannual variability in recent oceanic uptake of atmospheric carbon dioxide.
440 *Nature*, 396(6707), 155–159.
- 441 Li, H., & Ilyina, T. (2018). Current and future decadal trends in the oceanic carbon
442 uptake are dominated by internal variability. *Geophysical Research Letters*,
443 45(2), 916–925.
- 444 Li, H., Ilyina, T., Müller, W. A., & Landschützer, P. (2019). Predicting the variable
445 ocean carbon sink. *Science advances*, 5(4), eaav6471.
- 446 Li, H., Ilyina, T., Müller, W. A., & Sienz, F. (2016). Decadal predictions of the
447 north atlantic CO₂ uptake. *Nature communications*, 7(1), 1–7.
- 448 Lovenduski, N. S., Bonan, G. B., Yeager, S. G., Lindsay, K., & Lombardozzi, D. L.
449 (2019). High predictability of terrestrial carbon fluxes from an initialized
450 decadal prediction system. *Environmental Research Letters*, 14(12), 124074.
- 451 Lovenduski, N. S., Yeager, S. G., Lindsay, K., & Long, M. C. (2019). Predicting
452 near-term variability in ocean carbon uptake. *Earth System Dynamics (On-*
453 *line)*, 10(1).

- 454 Marotzke, J., Müller, W. A., Vamborg, F. S., Becker, P., Cubasch, U., Feldmann, H.,
455 ... others (2016). MiKlip: A national research project on decadal climate pre-
456 diction. *Bulletin of the American Meteorological Society*, *97*(12), 2379–2394.
- 457 Mauritsen, T., Bader, J., Becker, T., Behrens, J., Bittner, M., Brokopf, R., ... oth-
458 ers (2019). Developments in the MPI-M Earth System Model version 1.2
459 (MPI-ESM1.2) and its response to increasing CO₂. *Journal of Advances in*
460 *Modeling Earth Systems*, *11*(4), 998–1038.
- 461 Merryfield, W. J., Baehr, J., Batté, L., Becker, E. J., Butler, A. H., Coelho, C. A.,
462 ... others (2020). Current and emerging developments in subseasonal to
463 decadal prediction. *Bulletin of the American Meteorological Society*, *101*(6),
464 E869–E896.
- 465 Park, J.-Y., Stock, C. A., Dunne, J. P., Yang, X., & Rosati, A. (2019). Seasonal to
466 multiannual marine ecosystem prediction with a global Earth system model.
467 *Science*, *365*(6450), 284–288.
- 468 Park, J.-Y., Stock, C. A., Yang, X., Dunne, J. P., Rosati, A., John, J., & Zhang, S.
469 (2018). Modeling global ocean biogeochemistry with physical data assimila-
470 tion: a pragmatic solution to the equatorial instability. *Journal of Advances in*
471 *Modeling Earth Systems*, *10*(3), 891–906.
- 472 Peters, G. P., Le Quéré, C., Andrew, R. M., Canadell, J. G., Friedlingstein, P., Ily-
473 ina, T., ... others (2017). Towards real-time verification of CO₂ emissions.
474 *Nature Climate Change*, *7*(12), 848–850.
- 475 Rayner, N., Parker, D. E., Horton, E., Folland, C. K., Alexander, L. V., Rowell, D.,
476 ... Kaplan, A. (2003). Global analyses of sea surface temperature, sea ice,
477 and night marine air temperature since the late nineteenth century. *Journal of*
478 *Geophysical Research: Atmospheres*, *108*(D14).
- 479 Rödenbeck, C., Bakker, D. C., Gruber, N., Iida, Y., Jacobson, A. R., Jones, S., ...
480 others (2015). Data-based estimates of the ocean carbon sink variability—
481 first results of the surface ocean pCO₂ mapping intercomparison (SOCOM).
482 *Biogeosciences*, *12*, 7251–7278.
- 483 Ropelewski, C. F., & Halpert, M. S. (1987). Global and regional scale precipitation
484 patterns associated with the El Niño/Southern Oscillation. *Monthly weather*
485 *review*, *115*(8), 1606–1626.
- 486 Roy, T., Bopp, L., Gehlen, M., Schneider, B., Cadule, P., Frölicher, T. L., ... Joos,

- 487 F. (2011). Regional impacts of climate change and atmospheric CO₂ on fu-
488 ture ocean carbon uptake: A multimodel linear feedback analysis. *Journal of*
489 *Climate*, 24(9), 2300–2318.
- 490 Séférian, R., Berthet, S., & Chevallier, M. (2018). Assessing the decadal predictabil-
491 ity of land and ocean carbon uptake. *Geophysical Research Letters*, 45(5),
492 2455–2466.
- 493 Séférian, R., Berthet, S., Yool, A., Palmiéri, J., Bopp, L., Tagliabue, A., . . . others
494 (2020). Tracking improvement in simulated marine biogeochemistry between
495 CMIP5 and CMIP6. *Current Climate Change Reports*, 6, 95–119.
- 496 Séférian, R., Bopp, L., Gehlen, M., Swingedouw, D., Mignot, J., Guilyardi, E., &
497 Servonnat, J. (2014). Multiyear predictability of tropical marine productivity.
498 *Proceedings of the National Academy of Sciences*, 111(32), 11646–11651.
- 499 Smith, D. M., Cusack, S., Colman, A. W., Folland, C. K., Harris, G. R., & Murphy,
500 J. M. (2007). Improved surface temperature prediction for the coming decade
501 from a global climate model. *science*, 317(5839), 796–799.
- 502 Spring, A., & Ilyina, T. (2020). Predictability horizons in the global carbon cycle
503 inferred from a perfect-model framework. *Geophysical Research Letters*, 47(9),
504 e2019GL085311.
- 505 Swart, N. C., Cole, J. N., Kharin, V. V., Lazare, M., Scinocca, J. F., Gillett, N. P.,
506 . . . others (2019). The Canadian Earth System Model version 5 (CanESM5.
507 0.3). *Geoscientific Model Development*, 12(11), 4823–4873.
- 508 UNFCCC, V. (2015). Adoption of the paris agreement. i: proposal by the president
509 (draft decision). *United Nations Office, Geneva (Switzerland)*.
- 510 Watanabe, M., Tatebe, H., Koyama, H., Hajima, T., Watanabe, M., & Kawamiya,
511 M. (2020). Importance of El Niño reproducibility for reconstructing historical
512 CO₂ flux variations in the equatorial Pacific. *Ocean Science Discussions*, 2020,
513 1–21. Retrieved from <https://os.copernicus.org/preprints/os-2020-32/>
514 doi: 10.5194/os-2020-32
- 515 Yeager, S., Danabasoglu, G., Rosenbloom, N., Strand, W., Bates, S., Meehl, G., . . .
516 others (2018). Predicting near-term changes in the earth system: A large
517 ensemble of initialized decadal prediction simulations using the Community
518 Earth System Model. *Bulletin of the American Meteorological Society*, 99(9),
519 1867–1886.

- 520 Zeng, N., Mariotti, A., & Wetzel, P. (2005). Terrestrial mechanisms of interannual
521 CO₂ variability. *Global biogeochemical cycles*, *19*(1).
- 522 Zeng, N., Yoon, J.-H., Vintzileos, A., Collatz, G. J., Kalnay, E., Mariotti, A., ...
523 Lord, S. (2008). Dynamical prediction of terrestrial ecosystems and the global
524 carbon cycle: A 25-year hindcast experiment. *Global Biogeochemical Cycles*,
525 *22*(4).

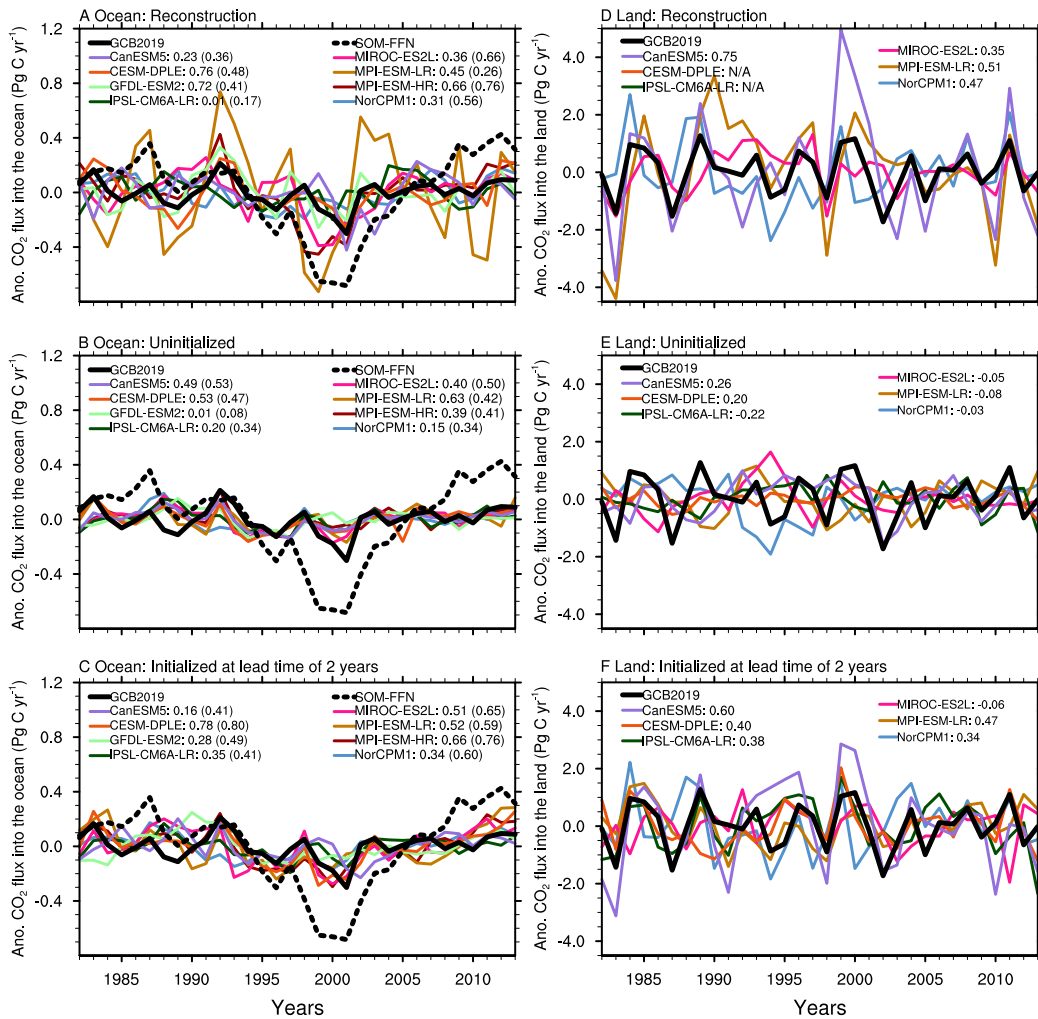


Figure 1. Time series of the global anomalous CO₂ flux relative to the climatological mean in each modeling system into the ocean (left) and land (right) from reconstruction (top), uninitialized simulation, (middle) and initialized retrospective prediction (bottom) simulations at lead time of 2 years. The long-term linear trends are removed for all the time-series. Left panels include available observation-based estimates from SOM-FFN. Numbers on the legends show the correlations relative to GCB and correlations relative to SOM-FFN data based estimates of the CO₂ flux into the ocean (shown in brackets). Outputs for air-land CO₂ fluxes from the reconstruction simulation were not available from IPSL-CM6A-LR and CESM-DPLE.

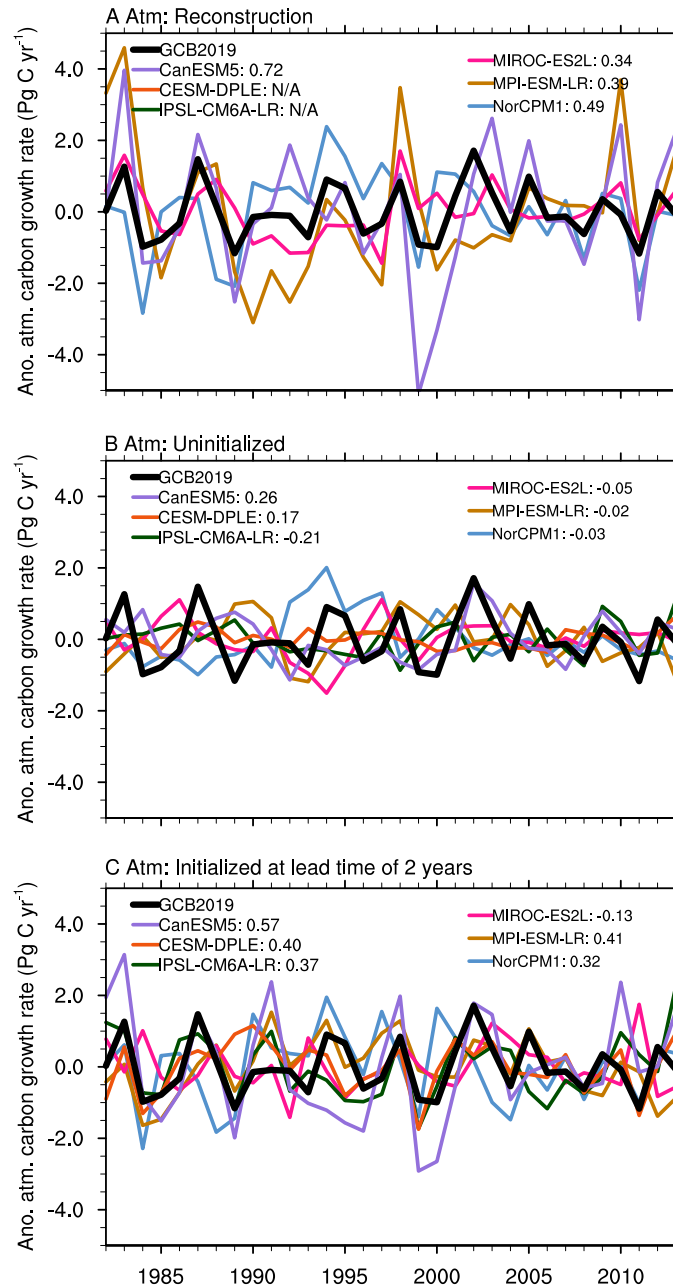


Figure 2. Time series of the anomalous atmospheric carbon growth rate due to natural variations of the ocean and land carbon sinks, represented by the reverse sign of the detrended land and ocean carbon sinks from reconstruction (top), uninitialized simulation, (middle) and initialized retrospective prediction (bottom) simulations at lead time of 2 years. Numbers on the legends show the correlations relative to GCB. Outputs for air-land CO_2 fluxes from the reconstruction simulation were not available from IPSL-CM6A-LR and CESM-DPLE, preventing the computation of the anomalous atmospheric carbon growth rates in these systems.

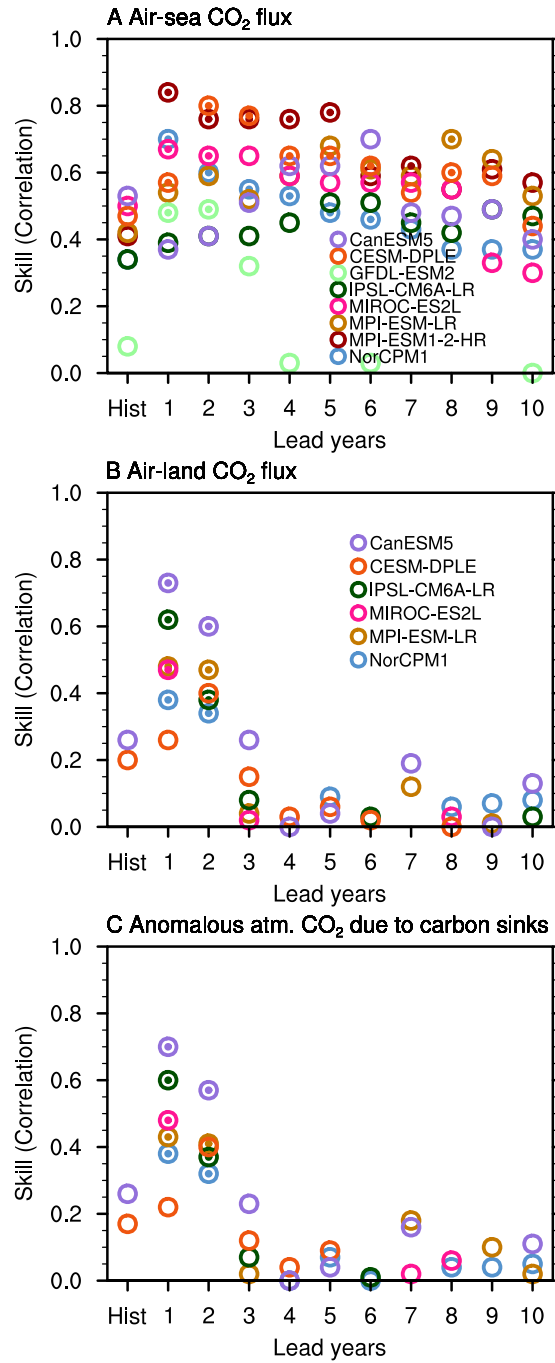


Figure 3. Predictive skill of the detrended CO₂ flux into the ocean (a), CO₂ flux into the land (b), and variations in the inferred atmospheric CO₂ growth (c). Predictive skill is quantified as anomaly correlation coefficients of the model simulations with the SOM-FFN observation-based product for the air-sea CO₂ fluxes (a), and with GCB2019 for the air-land CO₂ flux and anomalous atmospheric CO₂ due to carbon sinks. Significantly improved predictive skill at 95% level for initialized over uninitialized simulations are marked with filled dots, p-values given in Table S2. Note that GFDL-ESM2 and MIROC-ES2L hindcasts start earliest from year 1980, so from lead year 4 the time period is shorter than 1982-2013.

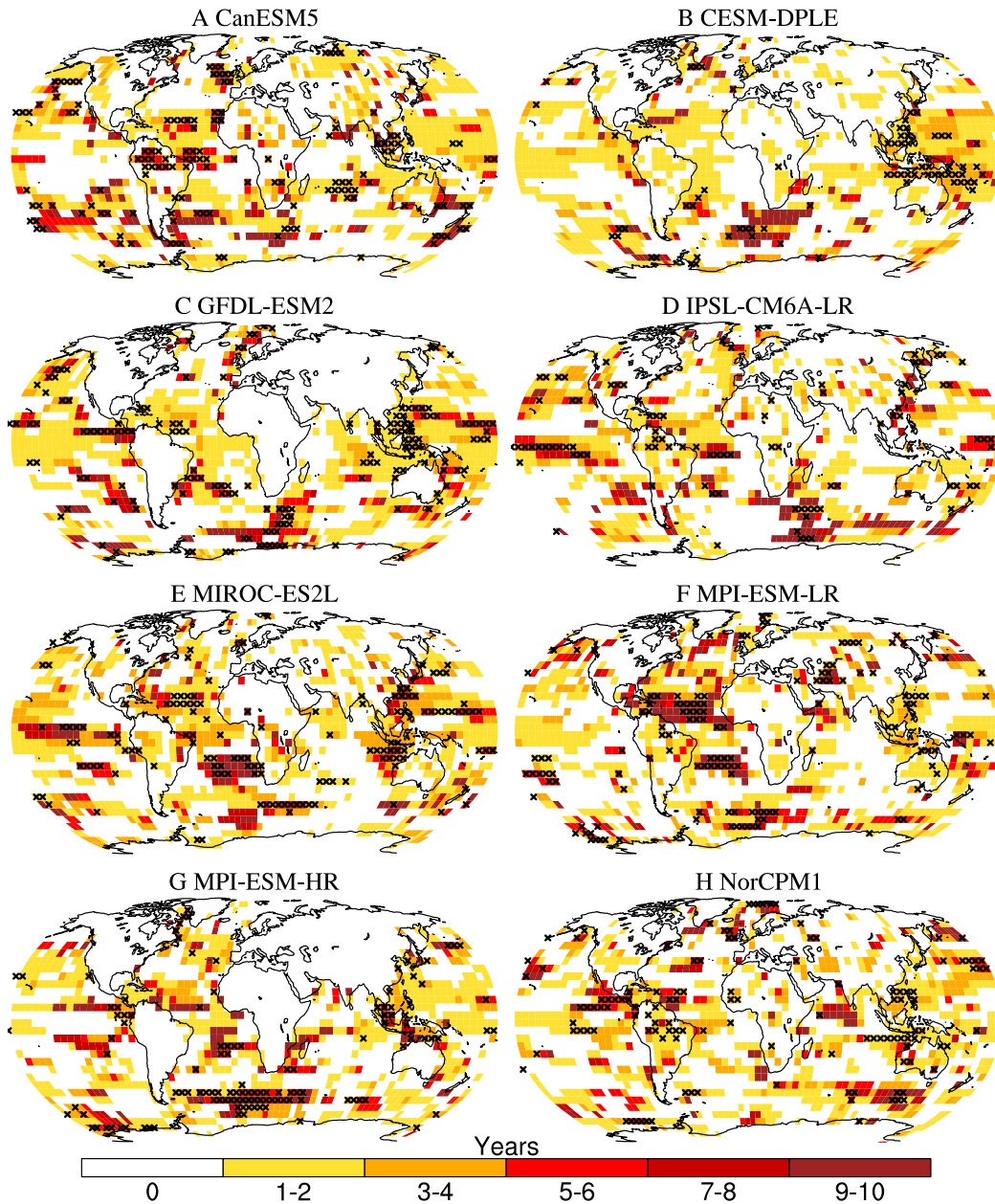


Figure 4. Predictability horizon of the detrended CO₂ flux into the ocean and the land, represented by the lead years with improved predictive skill due to initialization, i.e., when correlations in the initialized simulations are larger than 0 and also larger than those in the uninitialized simulations. Skill is quantified with anomaly correlation coefficient for the period 1982-2013. Predictive skill of the air-sea CO₂ flux gained due to initialization is assessed against SOM-FFN, whereas for the air-land CO₂ flux it is assessed against GCB. Crosses show significance at 95% level for the first 2 years. Note that GFDL-ESM2 and MIROC-ES2L hindcasts start earliest from year 1980, so from lead year 4 the time period is shorter than 1982-2013.